Optimized conditions for glycine-nitrate-based solution combustion synthesis of $LiNi_{0.5}Mn_{1.5}O_4$ as a high-voltage cathode material for lithium-ion batteries

Chunyu Zhu [a], Tomohiro Akiyama [a]*

[a]Center for Advanced Research of Energy & Materials, Hokkaido University, Sapporo 060-8628, Japan

*Corresponding author: Tel.: +81-11-706-6842; Fax: +81-11-726-0731.

E-mail address: takiyama@eng.hokudai.ac.jp (Tomohiro Akiyama)

Abstract

This paper describes the glycine-nitrate-based solution combustion synthesis of $LiNi_{0.5}Mn_{1.5}O_4$ as a high-voltage cathode material for lithium-ion batteries. The morphology, size, and crystallinity of the products were dependent on the synthesis conditions like glycine amount and calcination temperature and duration, as investigated in particular by X-ray diffraction and scanning electron microscopy, which likewise influenced their electrochemical properties. The electrochemical performance was characterized by galvanostatic charge-discharge cycling. The product obtained at a glycine/nitrate ratio of 1, which was calcined at 800 ºC for 24 h, indicated the best charge-discharge cycling performance. The sample showed an initial discharge capacity of 124.9 mAh/g and could retained 97.20% of the capacity after 50 cycles at a charge-discharge rate of 1 C. The sample also exhibited a good high-rate capability, indicating a high discharge capacity of 98 mAh/g at a rate of 10 C.

Keywords: combustion synthesis, lithium ion battery, $LiNi_{0.5}Mn_{1.5}O_4$, cathode material

1. Introduction

Much attention has been paid to the spinel $LiNi_{0.5}Mn_{1.5}O_4$ (LNMO) as a promising cathode material for lithium-ion batteries (LIBs) because of its high reversible capacity, low cost, and nontoxicity. LNMO has a high working voltage of around 4.7 V vs. Li^+/Li, and an energy density of 650 Wh/g, which is enhanced by 20% and 30% in comparison to conventional $LiCoO_2$ and $LiFePO_4$, respectively. Therefore, LIBs using LNMO as positive electrode are expected to provide higher power/energy density. [1, 2]

As the electrochemical properties of an electrode are determined by the phase, purity, structure, size, and morphology of the material, a number of efforts have been devoted to develop synthetic routes to obtain high-purity LNMO with optimized microstructures and suitable size that enable an improved performance. Generally, different preparation methods, such as the solid state method [3], coprecipitation method [4-7], sol-gel preparation [8, 9], the molten salt method [10], hydrothermal synthesis [11] and others, have been used to produce LNMO with different morphologies and particle sizes ranging from nanometers to microns. Although LNMO with good electrochemical performance may be synthesized by these methods, some unfavorable factors, in particular the high cost of the raw materials, a complex processing, and the appearance of impurity phases (such as NiO or $Li_xNi_{1-x}O$), have constrained their application for the commercial production of LNMO.

Solution combustion synthesis (SCS) is a promising alternative method. It is a combustion synthesis process based on a highly exothermic, self-sustaining reaction generated by heating a solution mixture of aqueous metal salts and fuels, such as urea, citric acid, or glycine. This approach has been used to synthesize a variety of compounds including binary and complex oxides, such as ferrites, spinels, and perovskites. This method not only yields nanosized products exhibiting large specific surface areas but also enables a uniform (homogeneous) doping of trace amounts of various elements in a single step. Several reports have been concerned with the solution combustion synthesis of cathode materials for LIBs, such as the glycine-based combustion synthesis of layered $LiMO_2$ and spinel-type $LiMn_2O_4$ [12-14]. The characteristics (including purity, structure, and size) of the SCS-derived oxides are typically determined by several synthetic parameters, such as the species of fuel and oxidizer reactants, the fuel-to-oxidizer ratio, and the subsequent sintering treatment after SCS. These

characteristics correspondingly influence their electrochemical properties as cathode materials in LIBs. However, there is no comprehensive study on glycine-nitrate-based SCS of LNMO. Therefore, in this paper, we describe the optimized production conditions for such a glycine-nitrate-based SCS of LNMO and, additionally, provide the electrochemical characterization of the material to be applied as cathode in lithium-ion batteries.

2. Experimental

Materials preparation and characterization: In a typical synthesis, lithium nitrate, nickel nitrate, and manganese nitrate in a molar ratio of Li/Ni/Mn = 1.1/0.5/1.5 (10% Li excess) were required for preparing 3 g of LNMO. These chemicals were sufficiently dissolved in distilled water in an alumina crucible, and the homogenous solutions were subsequently mixed with glycine fuel (to achieve a glycine to nitrate-ion ratio (G/N) in the range of 0.5 to 1.5) and magnetically stirred. The as-prepared solutions containing metal nitrates and glycine were heated on a hot plate while stirring to evaporate excess water until gels were obtained. The as-derived sol-gels in the crucibles were transferred to a lab-made combustion synthesis apparatus [14, 15], shown in Figure 1. The reactor was transferred to a heater which was pre-heated to and maintained at 400 ºC. The viscous sol-gel mixtures self-ignited under heating to produce voluminous ashes associated with the emission of large amounts of gases. The power of the heater was turned off as soon as the combustion reactions were observed and the reactor was cooled naturally inside of the heater. The temperature history during the combustion reaction was recorded. The apparatus consisted of a stainless-steel bin with a long vertical stainless-steel mesh chimney. This design enabled the safe removal of large amounts of gases as-released during the combustion reaction, while the products in form of ashes were remained in the reactor. The ash products were collected after the reaction and hand-milled roughly in a mortar-pestle.

To obtain high-purity LNMO as final products, the SCS-prepared precursors were subsequently calcined at 800 to 1000 ºC in ambient atmosphere and cooled naturally in the electronic furnace.

Powder X-ray diffraction (XRD, Rigaku Miniflex, Cu-Kα) was used to characterize the phase composition of the obtained materials. Scanning electron microscopy (SEM, JEOL, JSM-7400F) was used for the microscopic observation of the product morphology and size. The decompostion behavior of the SCS-derived precursors was investigated by a thermogravimetric (TG, Mettler Toledo) analyzer.

Electrochemical measurement: The electrochemical performance of the cathode materials were studied using a two-electrode Swagelok-type cell with a lithium metal anode as described in previous studies [14, 16]. The working electrodes consisted of the active oxide

material, conductive carbon (acetylene black), and polymer binder (polyvinylidene fluoride, PVDF) in a weight ratio of 8:1:1. The above cathode materials were mixed in N-methyl-2-pyrrolidone (NMP) to form slurries which were spread on an aluminum foil current collector. The coated electrodes were dried in vacuum at 110 ºC over night. The dried electrodes were punched into 10 mm disks. Metallic lithium disks of 10 mm in diameter were used as counter and reference electrode. The cell-assembly was carried out in an Ar-filled glove-box. An electrolyte of 1 M $LiPF_6$ in ethylene carbonate (EC)/dimethyl carbonate (DMC) (1:1 in volume) was used. The cells were galvanostatically charged and discharged between 3.3 and 4.9 V versus Li/Li^+ at room temperature using a battery tester (KIKUSUI, PFX2011). Cyclic voltammetry (CV) measurements were performed using a potentiostat/galvanostat apparatus (Autolab, PGSTAT128N).

3. Results and discussion

3.1 Solution combustion synthesis and thermal analysis

The fuel/oxidizer character can be evaluated by the calculation of the elemental stoichiometric coefficient ϕ, which is the ratio between the total valencies of fuels and the total valencies of nitrates based on the assumption described in reference [17]. Here, ϕ = 1 indicates a stoichiometric mixture, ϕ < 1 indicates an insufficient fuel condition whereas ϕ > 1 means an excess fuel condition. In this study, G/N = 0.5, 1.0, and 1.5 results in ϕ values of 0.9, 1.8, and 2.7, respectively. Figure 1 shows the temperature history of the combustion reactions at different G/N ratios. The sol-gel mixture with G/N = 0.5 self-ignited at around 145 ºC and subsequently showed a steep temperature rise to a maximum temperature of around 240 ºC. This mixture showed a relatively vigorous and complete combustion reaction between the glycine fuel and nitrite oxidizers at near the stoichiometric condition. However, the fuel-rich sol-gel mixtures with G/N ratios of 1 and 1.5 ignited at around 240-260 ºC. The abundant fuel made the reactions start near the combustion temperature of glycine with air (the TG analysis of glycine combustion in air indicated a reaction at around 250 ºC). The combustion reactions at G/N = 0.5 and 1 quickly reached maximum temperatures of 240 ºC and 355 ºC, respectively, after ignition, and the samples were cooled down naturally as the power of the heater was turned off. However, at G/N = 1.5, after reaching the maximum combustion reaction temperature of 360 ºC, the sample showed a continuous temperature increase to more than 400 ºC, which was due to the burning of the large amount of excess glycine fuel.

Note that the use of a thermocouple can only reflect the temperature change of the whole system. The combustion flame temperature is determined by the fuel ratio. At G/N=0.5 (with ϕ=0.9, near the stoichiometric condition), the combustion reaction was the most intensive and sufficient which was estimated with the highest flame temperature. This was also confirmed by the steep and fast temperature increase as measured by a thermocouple. The combustion flame temperature could be higher than 1000 ^{o}C. [18] However, the measured maximum temperature using a thermocouple is not very high. This is because of that the combustion reaction started at a low temperature and the released heat was absorbed by the cooled apparatus. Furthermore, since that the combustion reaction at this condition was explosive, the reaction heat was dispersed quickly with the scattered powders. The high flame

temperature leaded to a reduction of Mn^{4+} to Mn^{3+}, and the yielded Mn^{3+}–O structure participated in the electrode redox reaction and in turn, resulted in the capacity at around 4.0 V, [3] which was discussed in the following part. However, as increasing the glycine amount to G/N=1 and 1.5, the abundant fuel made the reactions start near the combustion temperature of glycine with air, and the increased glycine could alleviate the combustion reaction with lowered flame temperature, so as to avoid the Li excess loss at high flame temperature.

A precise measurement of the combustion flame temperature using an optical spectrometer is needed in the future to clarify the combustion behavior of the nitrate-glycine combustion reactions at different fuel ratios.

TG analysis was used for characterizing the properties of the SCS-prepared precursors. Figure 2 shows the TG curves of the precursors which were obtained under air atmosphere at a heating rate of 10 ºC/min. Weight losses at ~250–400 ºC, which were caused by the decomposition and/or combustion of intermediate products such as carbonaceous residues, were found to be about 2.3%, 15.6%, and 3.3% for the precursors obtained at G/N = 0.5, 1, 1.5 respectively. At G/N = 0.5, the sample showed the lowest weight loss, indicating a sufficient combustion reaction between the glycine fuel and nitrate oxidizers at near the stoichiometric condition. At G/N = 1 and 1.5, it was expected that the SCS-derived precursors would show greater weight changes because of the insufficient combustion reactions at the fuel-rich conditions, which might leave a large amount of unreacted glycine or carbonaceous residues. However, the precursor obtained at G/N = 1.5 showed a weight loss of only 3.3%, compared with the sample obtained at G/N = 1 with a weight loss of 15.6%. This was because of that the sample produced at G/N = 1.5 had showed a continuous burning of excess fuel or carbonaceous residues after the combustion reaction, as confirmed by the temperature history in Figure 1. The TG results indicate that the formation of the final product LNMO requires an extra calcination step at temperatures above 400 ºC.

3.2 Structure and morphology analysis

Figure 3 shows the XRD patterns of the calcined products obtained by a heat treatment at 900 ºC for 10 h. The XRD patterns of the as-SCS-derived precursors were also presented for comparison, which revealed almost amorphous products. Figure 4 shows the XRD patterns of

the calcined products obtained at different heat treatment temperatures ranging from 800 to 1000 ºC for 10 h. All peaks of the calcined samples can be indexed according to a single phase of spinel-type structure with space group *Fd3m* (JCPDS card No.: 80-2162), thus indicating the successful synthesis of LNMO by SCS with a subsequent calcination treatment. Notably, no obvious peak characteristic for presence of $Li_xNi_{1-x}O$, that is close to the (400) peak of the nominal spinel structure of LNMO, was found in our SCS products. Such impurity phase have been frequently observed during the synthesis of LNMO [5].

The morphology and structural features of the SCS-prepared precursors, as well as of the calcined products, were characterized by SEM. Figure 5 shows the SEM images at different magnification for the SCS-derived precursors at different G/N ratios. The precursors obtained at G/N = 0.5 and 1.5 showed particle sizes of more than 10 μm. However, the particle size of the precursor obtained at G/N = 1 was smaller than 5 μm. The calcined products (900 ºC, 10 h) showed similar secondary particle sizes with the SCS-prepared precursors, as shown in Figure 6. The observation of the products at a large magnification indicated that the three samples were composed of agglomerated small primary particles in the range of around 500–1000 nm. Figure 7 shows the SEM images of the final products, which were calcined at different temperatures for the precursor obtained at G/N = 1. Clearly, these samples showed a grain growth with the increase of calcination temperature. At 800 ºC, the primary particle size was in the range of 100–500 nm, at 900 ºC, the size was 500–1000 nm, while at 1000 ºC, the grains were as large as more than 1 μm.

Since the electrochemical properties of cathode materials are significantly influenced by their purity, crystallinity, particle size, and morphology, the G/N ratio and calcination conditions (temperature and duration) become important parameters for obtaining the best product by SCS. Therefore, the electrochemical performance of the samples obtained at different conditions was evaluated to find an optimized product.

3.3 Electrochemical performance: effects of G/N ratio and calcination temperature

The electrochemical properties of the LNMO powders were investigated in Swagelok-type cells using a Li-disk as reference and counter electrode. All cells were galvanostatically cycled at a potential range of 3.3–4.9 V versus Li/Li^+ and a current density

of 1 C. Here, 1 C is defined as a full charge/discharge of the theoretical capacity in 1 h, and in this study 1 C corresponds to a current density of 140 mA/g for LNMO. Figure 8-(a) illustrates the charge-discharge cycling performance of the products obtained at G/N = 1, which were calcined at 800–1000 ºC for 10 h. The sample calcined at 900 ºC exhibited the largest reversible capacities during the 50 charge-discharge cycles. The initial discharge capacity was 116.5 mAh/g and, after 50 cycles, the sample showed a discharge capacity of 113.0 mAh/g. Figure 8-(b) shows the comparison of the charge-discharge cycling capacities of the products obtained at different fuel ratios with a calcination temperature of 900 ºC for 10 h. Obviously, the product obtained at G/N = 1 exhibited the highest charge-discharge capacities. Figure 8-(c) presents the charge-discharge curves of the most favorable sample (G/N = 1, calcined at 900 ºC for 10 h) at different cycles. Figure 8-(d) shows the charge-discharge profiles at the 50^{th} cycle of the above five samples. All curves indicated two distinct plateaus at around 4.7 V which can be attributed to the Ni^{2+}/Ni^{3+} and Ni^{3+}/Ni^{4+}redox couple. The short plateaus at around 4.0 V were regarded to be caused by the redox reaction of Mn^{3+}/Mn^{4+}. These were also confirmed by the cyclic voltammetry measurement as shown in the following part. The discharge capacities at the 50^{th} cycle were 109.7, 113.0, 108.4 mAh/g for the samples obtained at G/N = 1 and calcined at 800, 900, 1000 ºC for 10 h, respectively, while the capacities were 99.1 and 71.4 mAh/g for the samples obtained at G/N = 0.5 and 1.5, respectively. The cycling capacity retention efficiencies of these samples were 97.08%, 94.80%, 94.15%, 83.14%, and 71.90% in corresponding sequence. A comparison of the cycling performance is summarized in Table 1. The capacity proportions corresponding to the Ni^{2+}/Ni^{4+} and Mn^{3+}/Mn^{4+} reactions at plateaus of 4.7 V and 4.0 V, respectively, were calculated based on the first discharge curves (Table 1). It is reported that a high reaction/sintering temperature could induce a reduction of Mn^{4+} to Mn^{3+}, and a high Mn^{3+} ratio in the LNMO cathode material is unfavorable due to its corresponding low plateau at 4.0 V. [3, 19] This is because of that the capacity of a cathode material at a low voltage gives a low energy density of the battery. The calculated proportions of capacity above 4.4 V (the capacity according to the 4.7 voltage plateaus) were summarized in Table 1. It is noted that at the same sintering condition the sample prepared at G/N=0.5 indicated the highest Mn^{3+} ratio, which was caused by the vigorous combustion reaction at this condition with a very high

flame temperature. Furthermore, with the increase of calcination temperature to 1000 ^{o}C the sample showed a higher Mn^{3+} ratio due to the severe sintering effect.

As shown by the SEM morphology observations presented in Figure 5 and Figure 6, the particle size greatly changed in dependence of the G/N ratio. The sample obtained at G/N = 1 revealed a secondary particle size that was smaller than 5 μm. However, the samples prepared with G/N = 0.5 and 1.5 showed secondary particle sizes of more than 10 μm. This was the reason for the greatly reduced performance of the samples obtained at G/N = 0.5 and 1.5. The crystallinity and primary grain size of the product were influenced by the calcination temperature, and hence the electrochemical properties. As shown in Figure 7, with the increase of the calcination temperature at equal duration, the product showed an increased grain size. As mentioned above, at 800 ºC, the primary grain size was in the range of 100–500 nm, at 900 ºC, the size was 500–1000 nm, while at 1000 ºC, the size was as large as more than 1 μm, which was due to the sever sintering effect at the very high temperatures. The specimen obtained at 1000 ºC showed the worst performance among these three samples due to the strongly sintered large grains. Although the capacities for the 800 ºC-sample were smaller than the capacity of the sample calcined at 900 ºC during the measured 50 cycles, this sample showed a better capacity retention efficiency (97.08% at 800 ºC while 94.80% at 900 ºC). The crystallinity of the sample obtained at 800 ºC was worse than the one prepared at 900 ºC, however, it can be further increased by enlongating the calcination duration. Therefore, in the following section, we change the calcination duration to find an optimized product.

3.4 Electrochemical performance: effect of calcination duration

Figure 9 shows the XRD patterns of the samples prepared with G/N = 1 and calcined at 800 and 900 ºC for 24 h, in comparison with the samples calcined for 10 h. The samples calcined for 24 h showed the same diffraction patterns like the samples calcined for 10 h, thus indicating a single phase of spinel-type LNMO. The sample calcined at 800 ºC for 24 h showed an increased crystallinity compared with the one calcined for 10 h, inferred from the stronger peak intensity. Figure 10 shows SEM images of the samples calcined for 24 h, evidencing larger grain sizes than the samples calcined for 10 h. Figure 11 presents the cycling performance (discharge capacities) and charge-discharge curves of the samples

calcined for different durations. At 800 ºC, with the increase of the calcination duration from 10 h to 24 h, the sample showed better crystallinity along with a slightly increased grain size. The sample calcined at 800 ºC for 24 h showed the best cycling performance with an initial discharge capacity of 124.9 mAh/g and a capacity retention efficiency of 97.20%. However, the capacity of the sample calcined at 900 ºC for 24 h decreased quickly, and after 50 cycles, 88.80% of the initial capacity (117.7 mAh/g) was retained. Furthermore, comparison of the proportion of the capacities above 4.4 V indicated that the sample calcined at 800 ºC for 24 h showed the lowest Mn^{3+} ratio. However, when calcined at 900 ºC for 24 h, the sample showed increased Mn^{3+} ratio as compared with the sample calcined for 10 h. All of these illustrated a proper calcination condition of 800 ºC for 24 h.

Figure 12 shows the typical CV curves of cells with the LNMO cathodes. Two strong split peaks at around 4.7 V were observed, corresponding to redox reactions of Ni^{2+}/Ni^{3+} and Ni^{3+}/Ni^{4+}. A weak peak at around 4.0 V indicated to the redox couples of Mn^{3+}/Mn^{4+}. These were also confirmed in the charge-discharge profiles, which presented two separated plateaus at around 4.7 V and a small plateau at around 4.7 V.

Table 1 summarizes the discharge capacities and capacity retention of the samples obtained at different conditions. All these results indicate in mutual agreement that the best-suited product for the application as cathode materials in LIBs is LNMO calcined at 800 ºC for 24 h with a G/N ratio of 1.

To further investigate the rate capability of the LNMO sample, the cell (made of the sample calcined at 800 ºC for 24 h with a G/N ratio of 1) was galvanostatically charged at a current density of 1 C and discharged at different C-rates from 1 C to 10 C and then backed to 1 C. As shown in Figure 13, the plateau voltage and discharge capacity decreased gradually with the increase of the current rate. This is commonly due to the increase of electrode overpotential and internal ohmic drop at high rates. At 10 C rate, the sample still delivered a stable discharge capacity of 98 mAh/g and an operating discharge voltage at around 4 V. After 70 cycles of charge-discharge at increasing C rates, the electrode exhibited discharge capacity of around 122 mAh/g when the discharge C rate returned to 1 C.

4. Conclusions

In summary, the high-voltage cathode material of $LiNi_{0.5}Mn_{1.5}O_4$ to be applied in lithium ion batteries was synthesized by glycine-nitrate-based solution combustion synthesis. The effects of glycine amount, calcination temperature and calcination duration on the structure, morphology, size, and electrochemical properties of the products were investigated to find the optimized production conditions. The product which was obtained at a glycine/nitrate ratio of 1 and calcined at 800 ºC for 24 h showed the best charge-discharge cycling performance. The sample delivered an initial discharge capacity of 124.9 mAh/g and retained 97.20% of the capacity after 50 cycles at a charge-discharge rate of 1 C. The sample also exhibited a good high-rate capability, which showed a high discharge capacity of 98 mAh/g at a rate of 10 C. The present results indicate that the glycine-nitrate SCS process is an attractive method for the fabrication of cost-effective cathode materials for lithium secondary batteries.

References

[1] T.-F. Yi, Y. Xie, M.-F. Ye, L.-J. Jiang, R.-S. Zhu, Y.-R. Zhu, Recent developments in the doping of $LiNi_{0.5}Mn_{1.5}O_4$ cathode material for 5 V lithium-ion batteries, Ionics, 17 (2011) 383-389.

[2] R. Santhanam, B. Rambabu, Research progress in high voltage spinel $LiNi_{0.5}Mn_{1.5}O_4$ material, Journal of Power Sources, 195 (2010) 5442-5451.

[3] Z. Zhu, H. Yan, D. Zhang, W. Li, Q. Lu, Preparation of 4.7V cathode material $LiNi_{0.5}Mn_{1.5}O_4$ by an oxalic acid-pretreated solid-state method for lithium-ion secondary battery, Journal of Power Sources, 224 (2013) 13-19.

[4] K.R. Chemelewski, D.W. Shin, W. Li, A. Manthiram, Octahedral and truncated high-voltage spinel cathodes: the role of morphology and surface planes in electrochemical properties, Journal of Materials Chemistry A, 1 (2013) 3347-3354.

[5] X. Zhang, J. Liu, H. Yu, G. Yang, J. Wang, Z. Yu, H. Xie, R. Wang, Enhanced electrochemical performances of $LiNi_{0.5}Mn_{1.5}O_4$ spinel via ethylene glycol-assisted synthesis, Electrochimica Acta, 55 (2010) 2414-2417.

[6] Z. Zhu, D. Zhang, H. Yan, W. Li, Qilu, Precise preparation of high performance spherical hierarchical LiNi0.5Mn1.5O4 for 5 V lithium ion secondary batteries, Journal of Materials Chemistry A, 1 (2013) 5492-5496.

[7] Y.-C. Jin, C.-Y. Lin, J.-G. Duh, Improving rate capability of high potential $LiNi_{0.5}Mn_{1.5}O_{4-x}$ cathode materials via increasing oxygen non-stoichiometries, Electrochimica Acta, 69 (2012) 45-50.

[8] N. Amdouni, K. Zaghib, F. Gendron, A. Mauger, C. Julien, Structure and insertion properties of disordered and ordered $LiNi_{0.5}Mn_{1.5}O_4$ spinels prepared by wet chemistry, Ionics, 12 (2006) 117-126.

[9] M.V. Reddy, H.Y. Cheng, J.H. Tham, C.Y. Yuan, H.L. Goh, B.V.R. Chowdari, Preparation of Li(Ni0.5Mn1.5)O4 by polymer precursor method and its electrochemical properties, Electrochimica Acta, 62 (2012) 269-275.

[10] L. Wen, Q. Lu, G. Xu, Molten salt synthesis of spherical $LiNi_{0.5}Mn_{1.5}O_4$ cathode materials, Electrochimica Acta, 51 (2006) 4388-4392.

[11] X. Huang, Q. Zhang, J. Gan, H. Chang, Y. Yang, Hydrothermal Synthesis of a Nanosized $LiNi_{0.5}Mn_{1.5}O_4$ Cathode Material for High Power Lithium-Ion Batteries, Journal of the Electrochemical Society, 158 (2011) A139-A145.

[12] C. Julien, C. Letranchant, M. Lemal, S. Ziolkiewicz, S. Castro-Garcia, Layered $LiNi_{1-y}Co_yO_2$ compounds synthesized by a glycine-assisted combustion method for lithium batteries, Journal of Materials Science, 37 (2002) 2367-2375.

[13] L. Li, Glycine-assisted combustion synthesis and electrochemical behavior of $LiNi_{0.5}Mn_{0.5}O_2$ nanoparticles under microwave irradiation, Journal of sol-gel science and technology, 53 (2010) 39-42.

[14] C. Zhu, A. Nobuta, G. Saito, I. Nakatsugawa, T. Akiyama, Solution combustion synthesis of $LiMn_2O_4$ fine powders for lithium ion batteries Advanced Powder Technology, DOI: 10.1016/j.apt.2013.05.015. (2013).

[15] C. Zhu, A. Nobuta, I. Nakatsugawa, T. Akiyama, Solution combustion synthesis of LaMO3 (M = Fe, Co, Mn) perovskite nanoparticles and the measurement of their electrocatalytic properties for air cathode, International Journal of Hydrogen Energy, 38 (2013) 13238-13248.

[16] C. Zhu, G. Saito, T. Akiyama, A new $CaCO_3$-template method to synthesize nanoporous manganese oxide hollow structures and their transformation to high-performance $LiMn_2O_4$ cathodes for lithium-ion batteries, Journal of Materials Chemistry A, 1 (2013) 7077-7082.

[17] S.R. Jain, K.C. Adiga, V.R. Pai Verneker, A new approach to thermochemical calculations of condensed fuel-oxidizer mixtures, Combustion and Flame, 40 (1981) 71-79.
[18] M. Lackner, Combustion Synthesis: Novel Routes to Novel Materials, Bentham Science Publishers. DOI: 10.2174/97816080515571100101, (2010).
[19] K. Kanamura, W. Hoshikawa, T. Umegaki Electrochemical Characteristics of $LiNi_{0.5}Mn_{1.5}O_4$ Cathodes with Ti or Al Current Collectors, Journal of The Electrochemical Society, 149 (2002) A339-A345.

Table 1. Capacity (Q) and cycling retention for the samples prepared at different conditions.

Sample	Q_{1st} (mAh g^{-1})	Proportion of Q_{1st} above 4.4 V (%)	Q_{50th} (mAh g^{-1})	Q_{max} (mAh g^{-1})	Q_{max} cycle No.	Capacity retention (%)
GN0.5-900 ºC-10h	117.3	83.02	99.1	119.2	4	83.14
GN1.5-900 ºC-10h	99.3	86.51	71.4	99.3	1	71.90
GN1-800 ºC-10h	113.0	85.76	109.7	113.0	1	97.08
GN1-900 ºC-10h	116.5	85.70	113.0	119.2	6	94.80
GN1-1000 ºC-10h	107.3	82.21	104.7	111.2	4	94.15
GN1-800 ºC-24h	124.9	86.84	121.4	124.9	1	97.20
GN1-900 ºC-24h	117.7	84.33	104.7	117.9	3	88.80

Figure 1. Temperature history of the combustion synthesis at different G/N ratios. 80 ºC was assumed as zero point for the data-log. The inset shows an image of the apparatus used for the combustion synthesis.

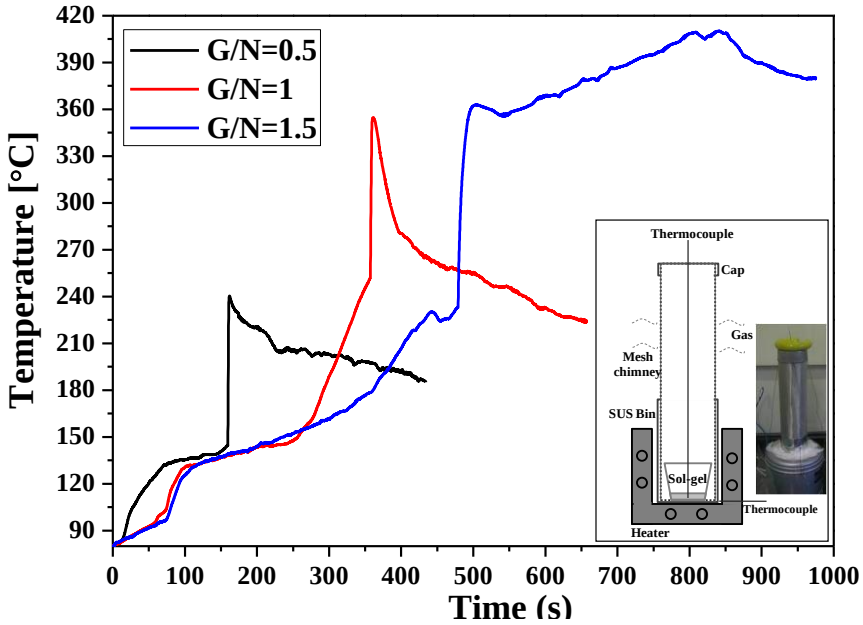

Figure 2. TG curves of the SCS-prepared precursors obtained under air atmosphere with a heating rate of 10 ºC/min.

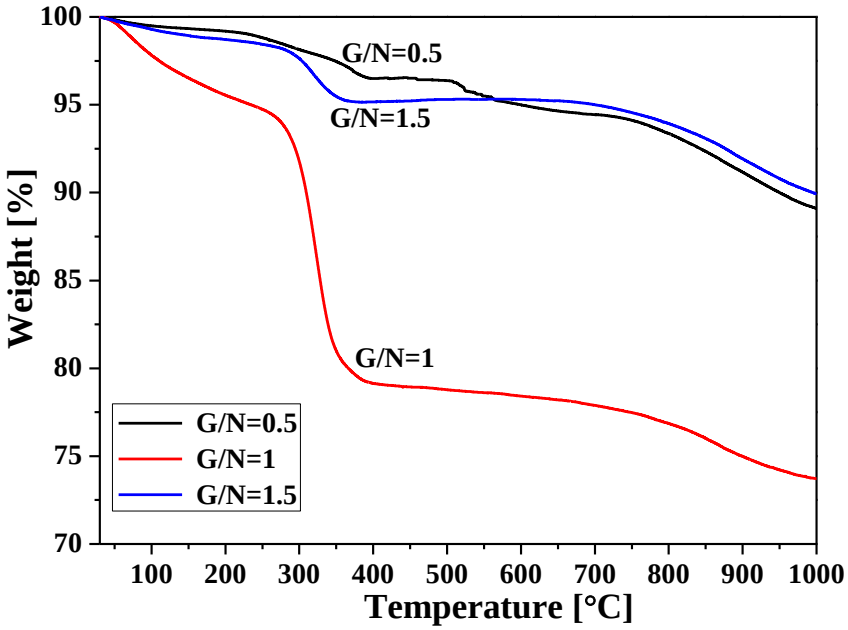

Figure 3. XRD patterns of the calcined products after a heat treatment at 900 ºC for 10 h with different G/N ratios, in comparison with the as-SCS-prepared precursors.

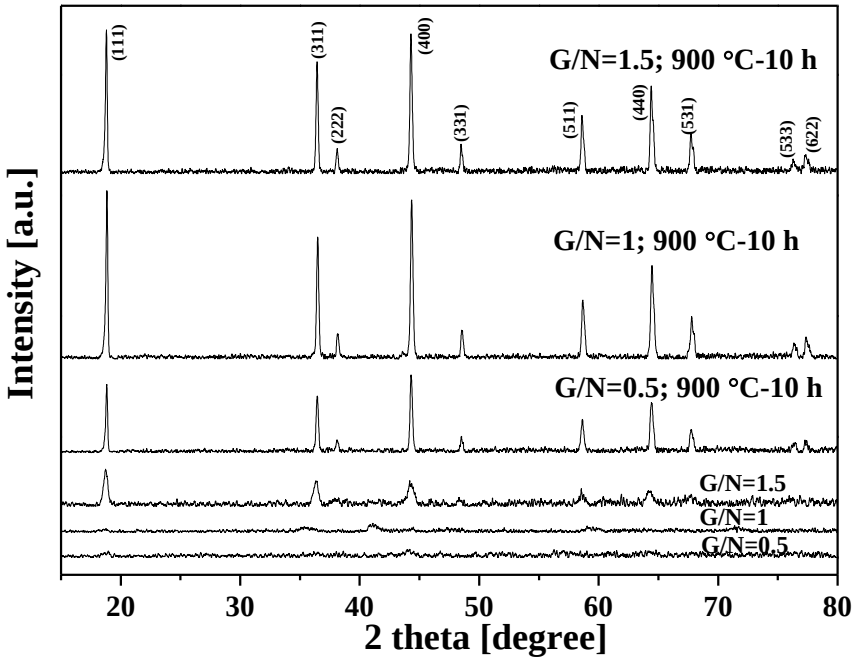

Figure 4. XRD patterns of the final products calcined at different temperatures with a G/N ratio of 1.

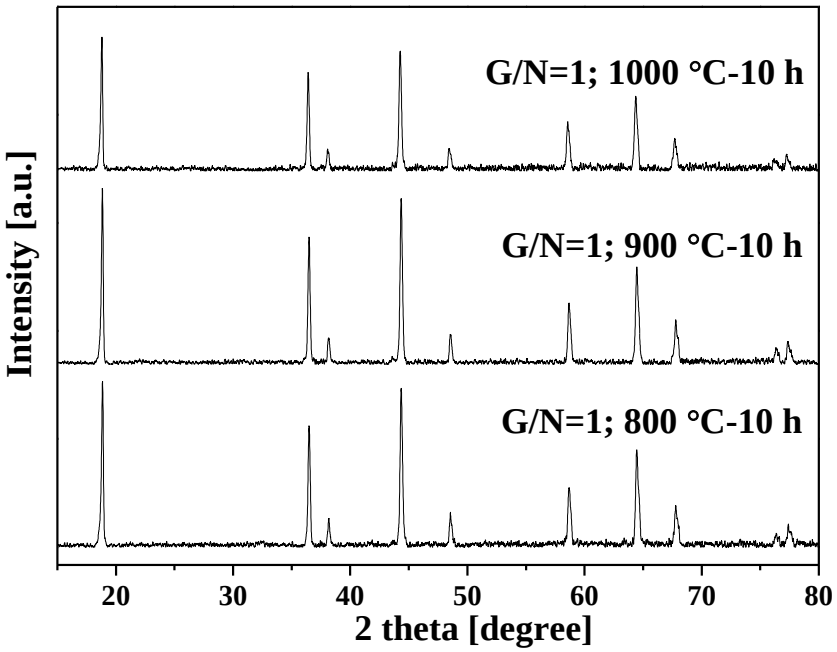

Figure 5. SEM images of the SCS-prepared precursors at different G/N ratios.

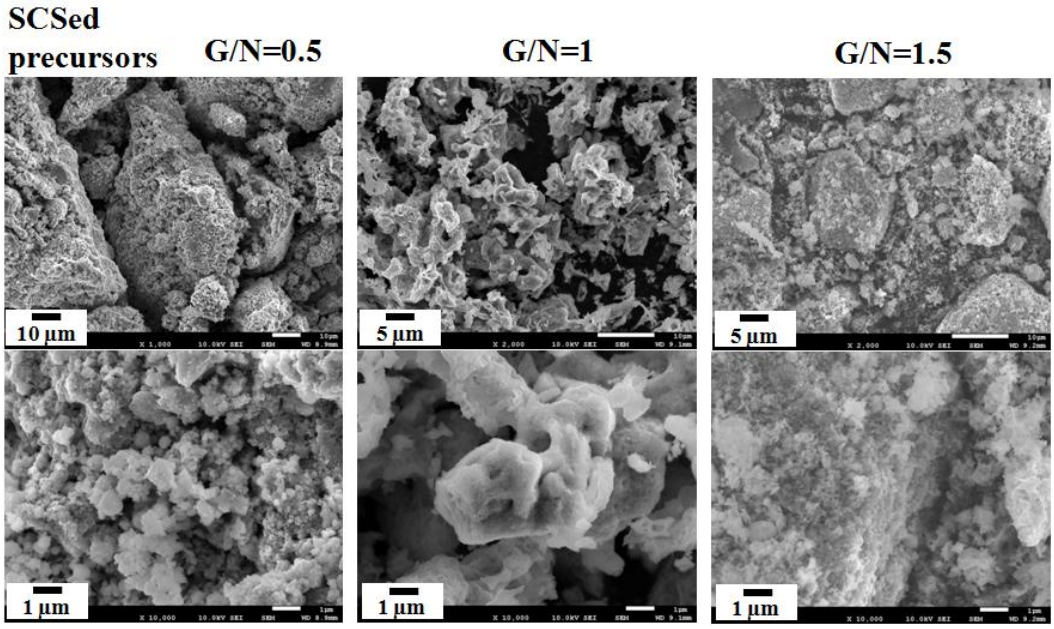

Figure 6. SEM images of the final products calcined at 900 °C for 10 h with different G/N ratios.

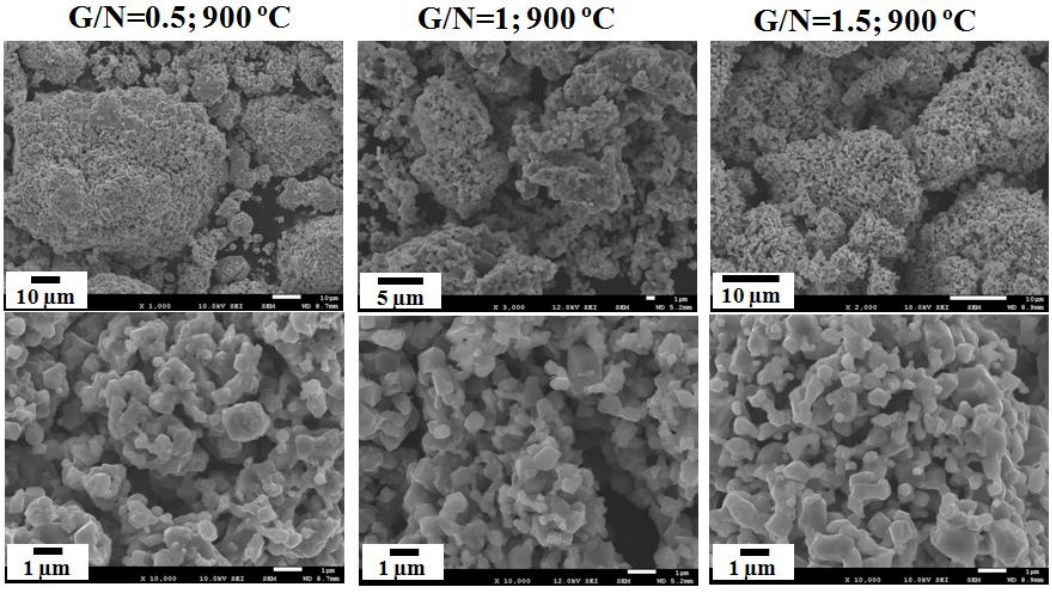

Figure 7. SEM images of the final products calcined at temperatures of 800, 900, and 1000 ºC for 10 h with G/N = 1.

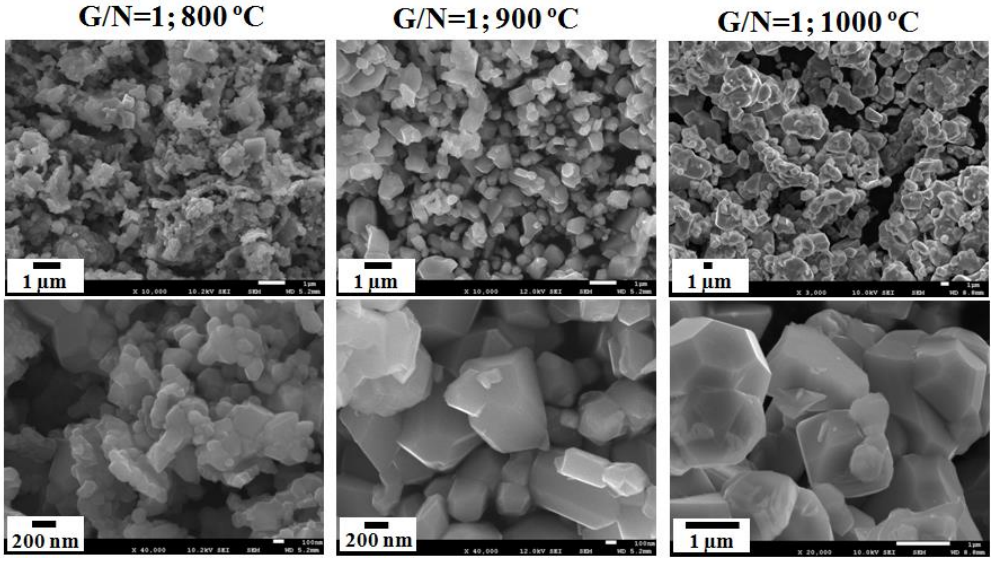

Figure 8. Cycling performance and charge-discharge curves of the calcined products with a calcination duration of 10 h. (a) at different calcination temperatures for G/N = 1; (b) at different G/N ratios for a calcination temperature of 900 ºC; (c) at different cycle numbers for the samples prepared with G/N = 1 and calcined at 900 ºC; (d) at the 50th cycle.

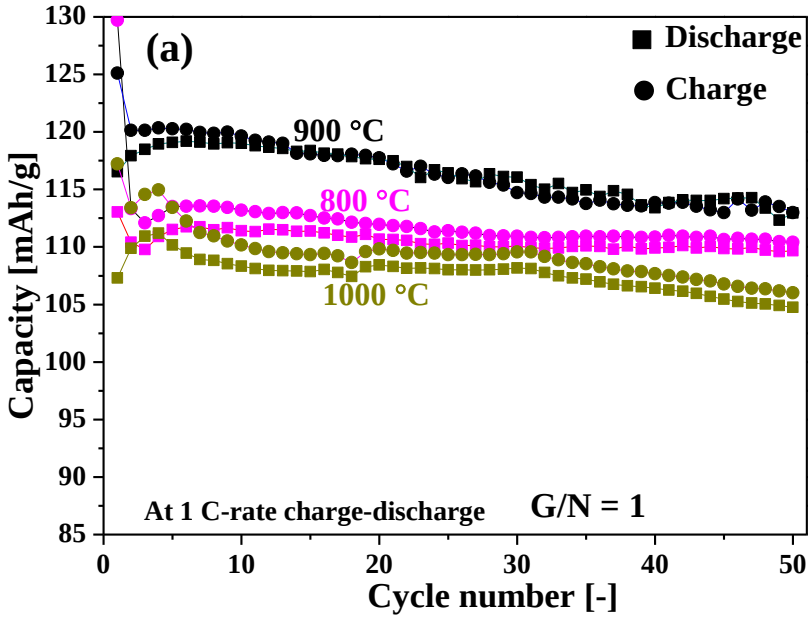

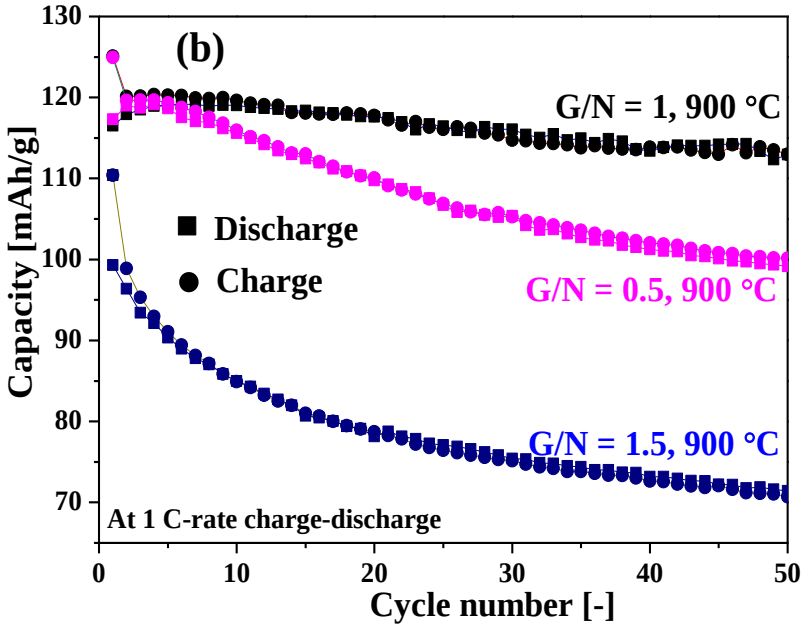

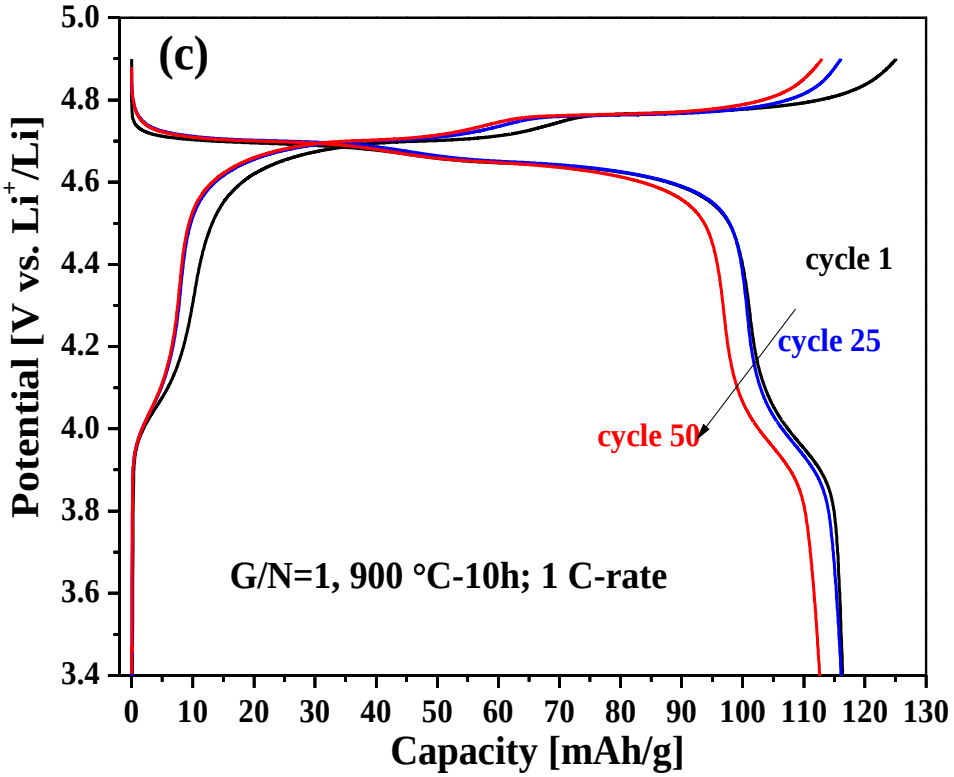
(c)
Potential [V vs. Li+/Li]
Capacity [mAh/g]
cycle 1
cycle 25
cycle 50
G/N=1, 900 °C-10h; 1 C-rate

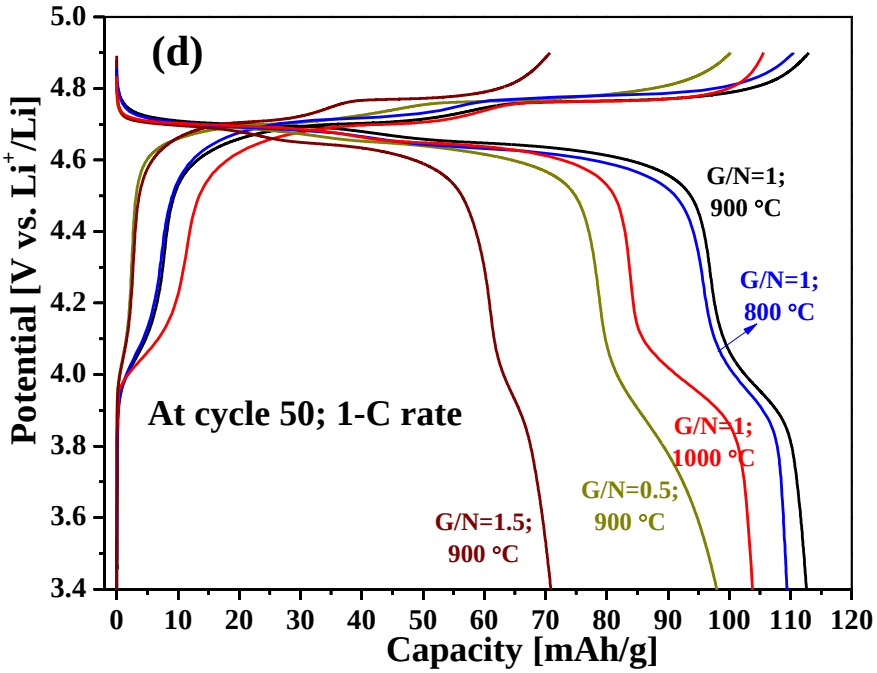
(d)
Potential [V vs. Li+/Li]
Capacity [mAh/g]
G/N=1;
900 °C
G/N=1;
800 °C
G/N=1;
1000 °C
G/N=0.5;
900 °C
G/N=1.5;
900 °C
At cycle 50; 1-C rate

Figure 9. XRD patterns of the final products, prepared with G/N = 1 and heat treated at different temperatures for different durations.

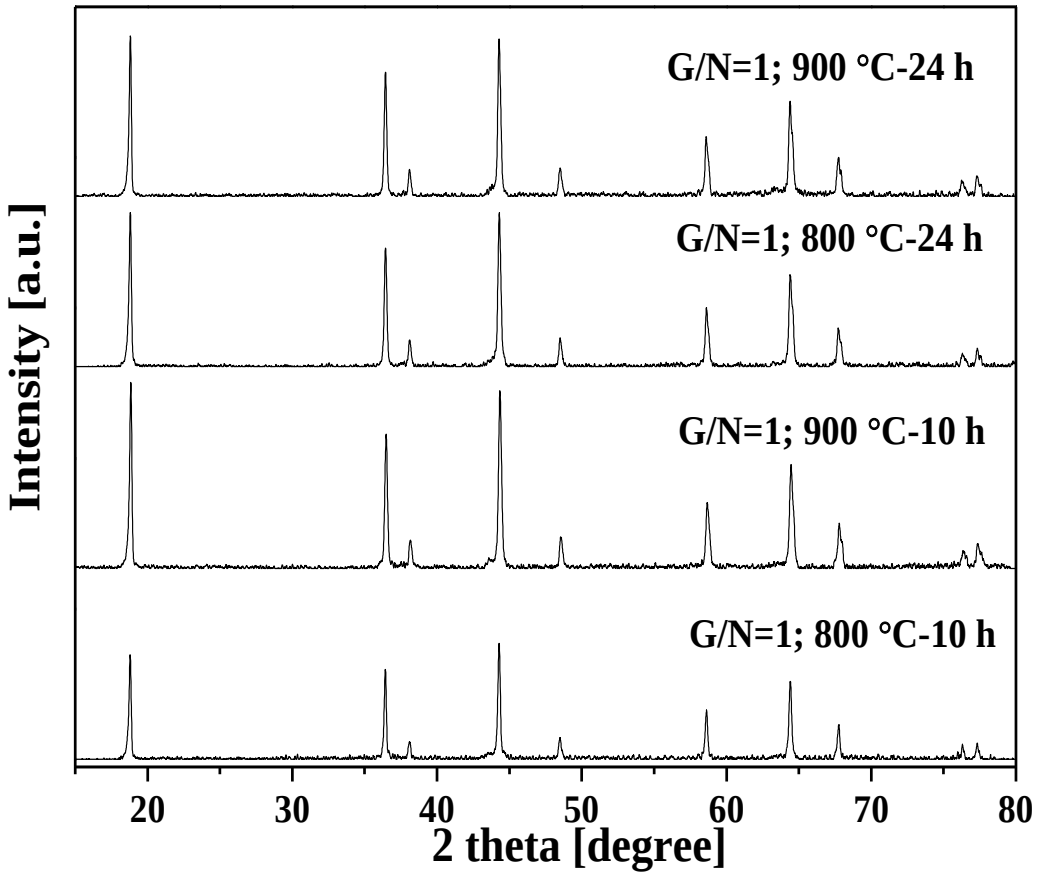

Figure 10. SEM images of the final products calcined at 800 ºC and 900 ºC for 24 h with G/N = 1.

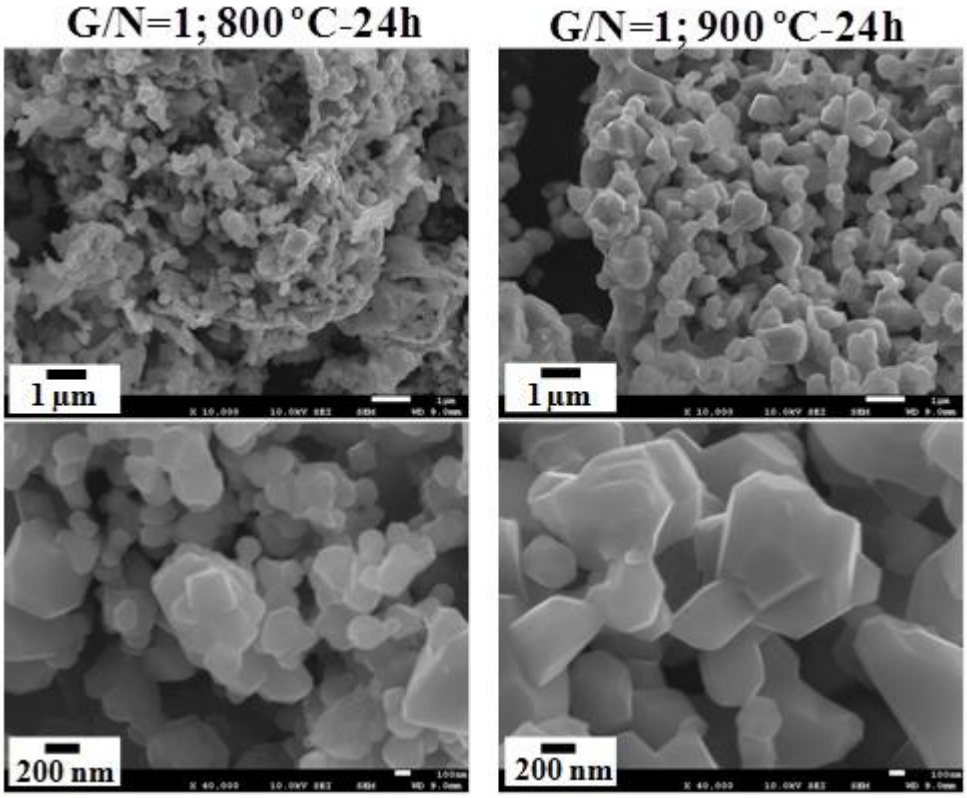

Figure 11. (a) Cycling performance of the final products calcined at different temperatures for different durations, and corresponding charge-discharge curves (b) during the first cycle and (c) during the 50th cycle.

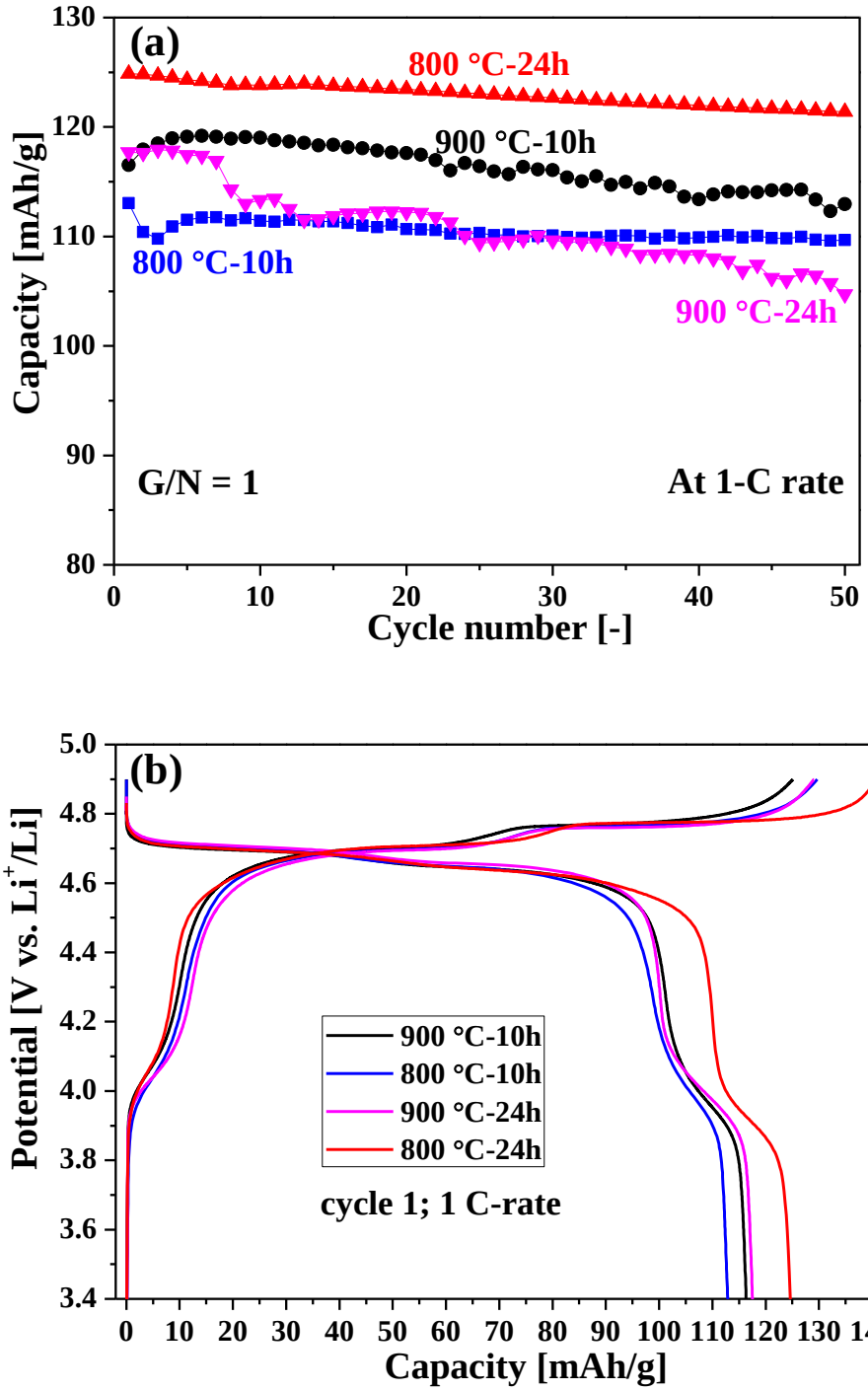

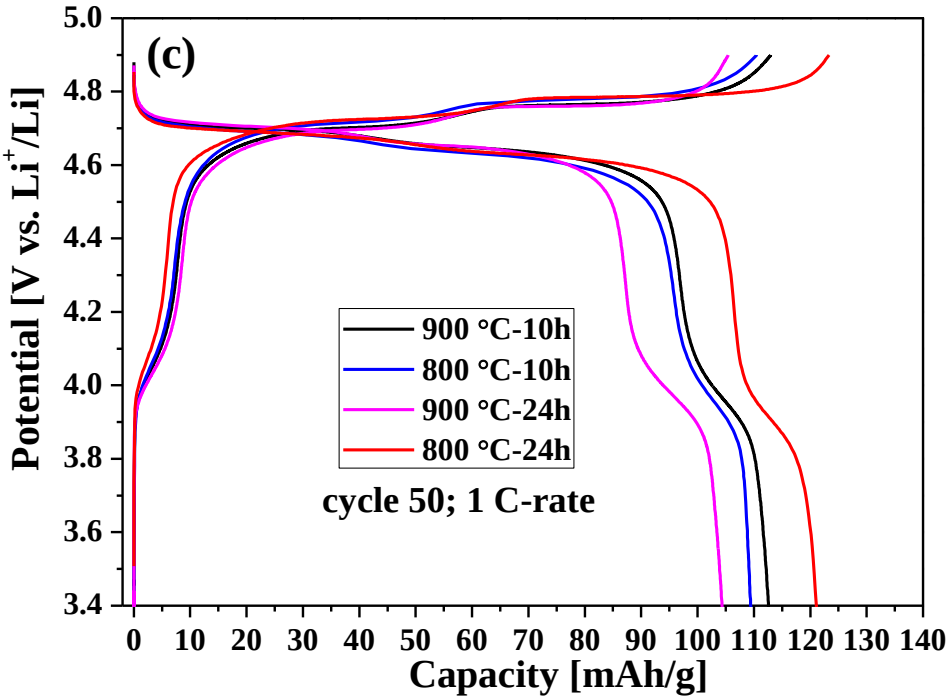
(c)
Potential [V vs. Li+/Li]
5.0
4.8
4.6
4.4
4.2
4.0
3.8
3.6
3.4
0 10 20 30 40 50 60 70 80 90 100 110 120 130 140
Capacity [mAh/g]
900 °C-10h
800 °C-10h
900 °C-24h
800 °C-24h
cycle 50; 1 C-rate

Figure 12. Typical CV curves of the electrodes made with the calcined cathode materials at a scan speed of 0.1 mV/s.

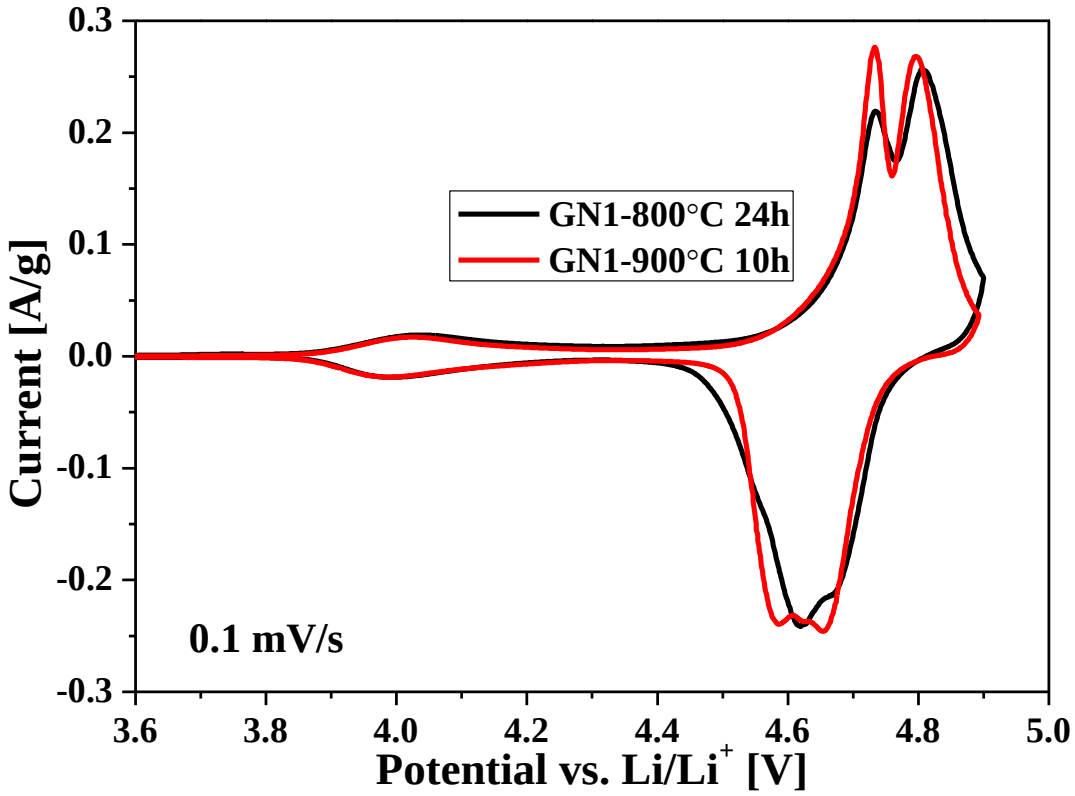

Figure 13. Discharge capacities and discharge profiles at different C rates for the product calcined at 800 °C for 24 h with a G/N ratio of 1.